Enhancing the Nanomaterial Bio-Interface by Addition of Mesoscale Secondary Features: Crinkling of Carbon Nanotube Films To Create Subcellular Ridges

Xing Xie,[†,#] Wenting Zhao,[‡,#] Hye Ryoung Lee,[§] Chong Liu,[‡] Meng Ye,[†] Wenjun Xie,[∥] Bianxiao Cui,[∥] Craig S. Criddle,[*,†] and Yi Cui[*,‡,⊥]

[†]Department of Civil and Environmental Engineering, Stanford University, 473 Via Ortega, Stanford, California 94305, United States, [‡]Department of Materials Science and Engineering, Stanford University, 476 Lomita Mall, Stanford, California 94305, United States, [§]Department of Electrical Engineering, Stanford University, 350 Serra Mall, Stanford, California 94305, United States, [∥]Department of Chemistry, Stanford University, 380 Roth Way, Stanford, California 94305, United States, and [⊥]Stanford Institute for Materials and Energy Sciences, SLAC National Accelerator Laboratory, 2575 Sand Hill Road, Menlo Park, California 94025, United States. [#]X.X. and W.Z. contributed equally.

ABSTRACT Biological cells often interact with their local environment through subcellular structures at a scale of tens to hundreds of nanometers. This study investigated whether topographic features fabricated at a similar scale would impact cellular functions by promoting the interaction between subcellular structures and nanomaterials. Crinkling of carbon nanotube films by solvent-induced swelling and shrinkage of substrate resulted in the formation of ridge features at the subcellular scale on both flat and three-dimensional substrates. Biological cells grown upon these crinkled CNT films had enhanced activity: neuronal cells grew to higher density and displayed greater cell polarization; exoelectrogenic micro-organisms transferred electrons more efficiently. The results indicate that crinkling of thin CNT films creates secondary mesoscale features that enhance attachment, growth, and electron transfer.

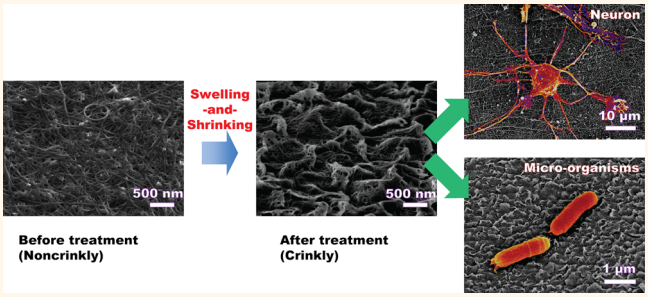

KEYWORDS: bio-interface · neuron · microbial fuel cells · coatings · solvent-based process

Biological cells sense and respond to local environmental conditions, including physical features such as nanowires, nanopillars, nanofibers, and nanotubes.[1,2] The presence of such features creates a "bio-interface" that can enhance cell adhesion and survival,[3−5] hinder cell migration and swimming,[6,7] guide cell polarization and alignment,[8−10] alter the structure of microbial biofilms,[11−13] and promote cell differentiation.[14,15] These properties are important for the performance of medical devices,[16,17] energy recovery devices such as microbial fuel cells,[18,19] and materials that resist biofouling.[12,20]

Length scale is a key consideration in the design of bio-interfaces, especially when using nanomaterials more than 2 orders of magnitude smaller than biological cells, such as carbon nanotubes (CNTs). Cells naturally make use of subcellular structures at the scale of tens to hundreds of nanometers in order to explore and communicate with their environment. Examples include filopodia in mammalian cells and flagella in bacteria.[21,22] Collagen fibers, and other components of the extracellular matrix (ECM), are also produced by cells at this same scale.[1] We therefore hypothesize that superior bio-interfaces can be created by addition of secondary features at the scale of subcellular structures, that is, tens to hundreds of nanometers. Accordingly, we developed a methodology for addition of a secondary structure to CNT films. CNTs are of particular

* Address correspondence to ccriddle@stanford.edu, yicui@stanford.edu.

Received for review August 31, 2014 and accepted November 21, 2014.

Published online November 21, 2014
10.1021/nn504898p

interest due to their distinctive electrical, thermal, and mechanical properties, their ease of application as coatings on diverse substrates, and their capacity to confer topographical cues.[23−26] In neural engineering, both homogeneous and micropatterned CNT-coated surfaces are known to support neuron attachment,[23,27] facilitate measurement of neuronal electrophysiology,[24,28,29] and guide formation of neuronal networks.[9,30] In microbial electrochemical systems, such as microbial fuel cells (MFCs), CNT-coated bioelectrodes promote both microbial colonization and collection of electrons.[18,19]

The morphology of a CNT thin film coating is typically determined by its fabrication process.[31] When these films are formed by direct growth, the CNTs align vertically away from the substrate.[27,32] When a solution coating process is used for fabrication of the CNT film, the CNTs lie flat upon the substrate following its contours.[18,33] Lithography-based methods enable manipulation of CNT film morphology at the micron scale, either by patterning of the catalyst for direct CNT growth or by patterning of an adhesion layer to guide CNT coating.[27,30] Other researchers have used drawing techniques to orient bundles of CNTs on substrates into micron-scale networks.[9] More recently, a stretching-based technique for surface topography manipulation has been applied onto CNT thin films to create micron-scale anisotropically wavy morphology.[34−36] All of the above methods for modification of CNT film morphology result in micron-scale features.

To improve the CNT bio-interface, secondary features that can connect to subcellular structures, such as filopodia in mammalian cells or flagella in bacteria,[21,22] are intriguing to test according to our hypothesis. The scale of these substructures can be classified as "mesoscale": less than the micron-scale features created by methods described above but larger than the nanometer diameters of individual CNTs. Topographical features at this intermediate scale have strong effects on bacterial colonization.[11] Methods for synthesis of mesoscale CNT features are currently lacking, and we know of no prior reports on the effects of mesoscale CNT structures upon the nanomaterial bio-interface. Here, we report a simple method for addition of mesoscale morphology to CNT thin films. We introduce mesoscale topography by crinkling CNT films on 2D and 3D substrates by solvent- or solution-based isotropic swelling and shrinking of the substrates. We then test the resulting bio-interfaces for growth of neuronal cells and exoelectrogenic micro-organisms.

RESULTS AND DISCUSSION

To add mesoscale morphology to CNT films, we begin by solution coating a substrate, such as polyurethane (PU), with a CNT thin film (Figure 1a). The coating layer is conformal and attaches strongly to the

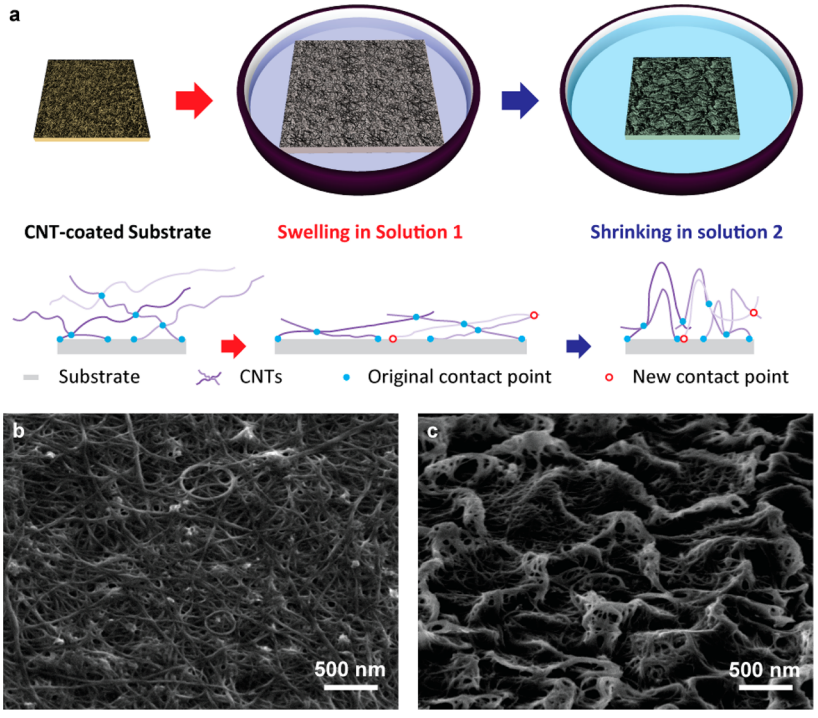

Figure 1. Creating mesoscale crinkly morphology on carbon nanotube (CNT) thin film. (a) Schematic of the two-step approach including expansion of CNT-coated substrate in a first solution (*e.g.*, acetone) and shrinkage in a second solution (*e.g.*, deionized water). Conformally coated CNTs irreversibly stretch with new contact points formed during the expansion of the substrate. When the substrate recovers to its original size, the CNT thin film buckles upward, forming mesoscale crinkly ridges. (b,c) Tilt (45°) scanning electron microscope images show the CNT thin film before (b) and after (c) the swelling-and-shrinking treatment.

substrate at multiple points of contact. The original topography is shown in Figure 1b. A simple and scalable two-step process is then used to generate mesoscale morphology. In the first step, the CNT-coated substrate is immersed in a liquid solvent, such as acetone or an acetone/water solution, and allowed to swell. Molecules from the liquid phase diffuse into gaps between polymer chains, and the substrate expands to a desired size. During expansion, individual CNTs slide through the CNT film, exposing more CNT surface to the substrate and creating additional points of contact (Figure 1a, middle). In step 2, the swollen substrate is immersed in a shrinkage solvent, such as deionized water. Molecules exit gaps in the polymer chains, and the substrate shrinks to its original dimensions.[37,38] Shrinkage releases strain, and instead of sliding back to initial flat film morphology, sections of the CNT thin film buckle upward between points of contact, creating a crinkly ridge morphology reminiscent of anticline folds in geology (Figure 1a, right).[39,40] The height of these ridges falls well within the mesoscale domain, ranging from tens of nanometers in width and hundreds of nanometers in height with lengths of up to a few microns (Figure 1c). To our knowledge, this is the first report of a methodology for creation of such morphology on CNT thin films. Further surface characterization by Fourier transform infrared spectroscopy (FT-IR) in attenuated total reflectance (ATR) mode and X-ray photoelectron spectroscopy (XPS) showed no detectable changes in surface functional groups upon such morphology generation by acetone treatment, and no detectable acetone residue was left after the shrinkage (Supporting Information Figure S1).

The dimensions of the crinkly morphology are tunable by controlling the swelling–shrinking process. For PU, expansion of polymer sheets proceeds to equilibrium within 2–4 h. Increasing the percentage of acetone in the swelling liquid increases the extent of expansion at equilibrium: an increase in acetone levels from 25 to 100% increases expansion from 3 to 21% (Figure 2a). Despite these large differences in the extent of expansion, swollen PU substrates subjected to different acetone treatments return to their original dimensions when submerged in deionized water for 4 h.

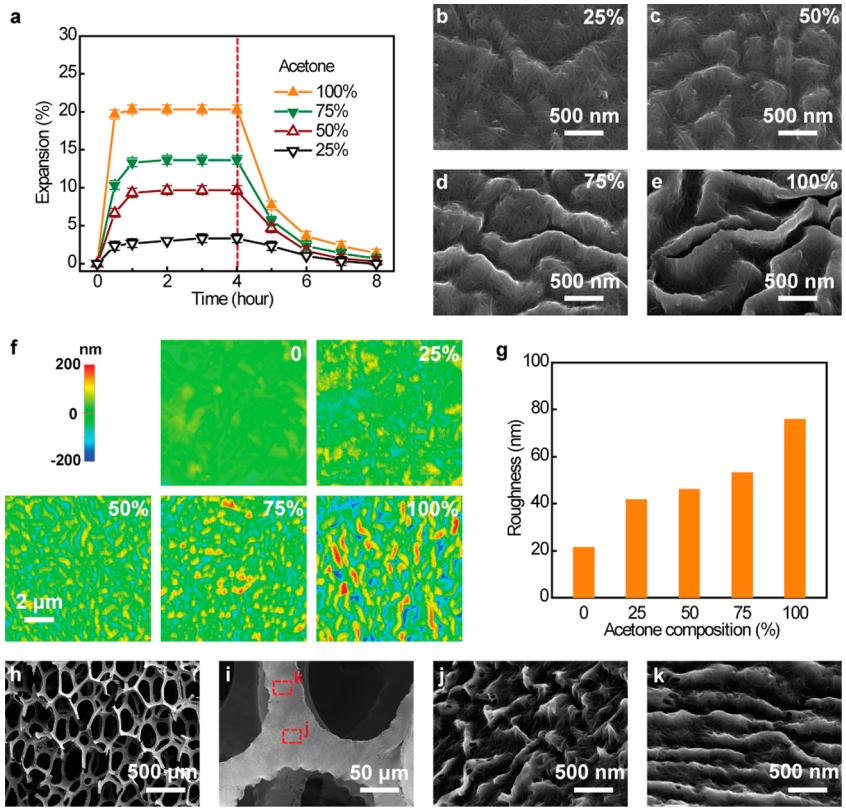

Figure 2. Controlled crinkling of CNT thin films on polyurethane (PU) sheet and sponge. (a) Dimension changes of the CNT-coated PU sheets during expansion in acetone–water solutions with varied acetone compositions (25, 50, 75, and 100%) followed by shrinking in deionized water. The dashed line indicates replacement of the acetone–water solution by deionized water. SEM images (b–e) and atomic force microscope (AFM) images (f) of the crinkly CNT thin films after the swelling-and-shrinking process. The percentages of acetone during expansion are noted in the top-right corner of the images. (g) Root mean square roughness of CNT thin films obtained by analyzing AFM images (f) with the XEI image processing software. (h) As-prepared CNT-coated PU sponge showing the 3D porous structure. (i–k) SEM images of CNT-coated PU sponge after swelling and shrinkage. The CNT thin film near the joint area of the sponge framework developed a randomly crinkly morphology (j), while the CNT thin film far away from the joint area revealed a more aligned wavy morphology with propagation of ridges normal to the orientation of the struts (k).

Both the extent of expansion and the initial expansion rate increase linearly with increasing acetone composition (Figure S2). Greater expansion results in more obvious crinkly morphology (Figure 2b–e). As acetone concentrations increase from 25 to 100%, the width of the ridges decreases from a few hundreds of nanometers to tens of nanometers, while the height increases to hundreds of nanometers. Such changes are uniform across a larger area (Figure S3). No CNTs peel off from the PU sheets during the swelling-and-shrinking process, indicating the strong van der Waals interaction between the CNTs and the PU substrate. To more accurately assess changes in ridge height at different acetone concentrations, we used atomic force microscopy (AFM) to measure the peak-to-peak amplitude of the crinkly morphology. Values increased from tens of nanometers at an acetone concentration of 25% to 300–500 nm in pure acetone, while the nontreated sample is relatively flat and uniform (Figure 2f). The root mean square roughness of the CNT film (Figure 2g) is consistent with this trend. Overall, these results indicate that the dimensions of the surface features can be tuned by controlled expansion of the PU sheet, and that the extent of expansion is a function of the composition of the liquid used to create swelling and time allowed for swelling.

The swelling-and-shrinking protocol is also easily applied to 3D substrates, such as sponge—a preferred scaffold for tissue engineering and for bioelectrodes. When a CNT-coated PU sponge (Figure 2h) was subjected to swelling and shrinking, crinkled CNT thin films formed on both the joints and struts (Figure 2i–k). Crinkling at joints resulted in randomly aligned ridges (Figure 2j), and crinkling on struts resulted in waves of parallel ridges aligned normal to the orientation of the strut (Figure 2k). A plausible explanation is that these features are the result of uneven strain distribution during sponge expansion: multidirectional strain at the joints generates the random crinkling morphology; unidimensional strain within the struts results in the aligned wavy morphology. To test this hypothesis, we clamped a coated PU sheet so as to constrain its expansion to a single direction (Figure S4a). Constrained expansion results in an aligned wavy morphology (Figure S4b), while unconstrained expansion retains a random morphology (Figure S4c). These differences are apparent in orientation maps that use color to differentiate surface feature angles. Aligned features appear as a single color (Figure S4d), whereas random alignments appear as a diversity of colors (Figure S4f), consistent with the angle distribution plots for these samples (Figure S4f).

CNTs are promising nanomaterials for nerve tissue regeneration,[41–43] but an effective bio-interface is critical for the actual performance. The crinkled ridge morphology of CNT thin films can potentially facilitate cellular interaction. Mammalian cells initiate interaction with nanoscale features, such as CNTs, through filopodia, substructures that are 100–300 nm in diameter and a few microns in length.[21] Crinkled CNT ridge features have comparable dimensions. To assess the potential use of crinkled CNT films as nanomaterial–neuron interfaces, we evaluated neuronal cell growth on CNT films with crinkled mesoscale topography.

Rat embryonic hippocampal neurons were plated on four different substrates, including a CNT-coated PU sheet treated with 100% acetone (CNT-PU-100), a CNT-coated PU sheet treated with 50% acetone (CNT-PU-50), an as-prepared CNT-coated PU sheet (CNT-PU-0), and a plain PU control. After 24 h *in vitro* culture, cells were stained by membrane marker CellMask Deep Red and nucleus marker Hoechst 33342 for morphology visualization and cell counting. Figure 3a shows the stained nucleus of cells attached to different substrates. The quantity of the nucleus marker is proportional to the number of cells. For control substrates, more cells attached to CNT-U-0. This is consistent with previous reports of enhanced cell attachment to CNT-coated surfaces.[27,30,44–46] After crinkly morphology generated by acetone treatment, even though the same number of cells was plated on all substrates, appreciably more cells attached to crinkled CNT films than to CNT-PU-0. Moreover, as the number of crinkled ridge features increased, more cells attached. Neuron density of CNT-PU-50 was 1.3-fold that of CNT-PU-0 and that of CNT-PU-100 was 1.7-fold greater than CNT-PU-0 (Figure 3d). A similar trend was observed for the cell membrane marker (Figure S5). These results indicate that addition of mesoscale morphology using crinkled CNT thin films facilitates the attachment and survival of neurons.

Another important aspect of neuronal interactions is polarization of shape. Neuronal cells are highly polarized with numerous protrusions. In a typical *in vitro* culture of hippocampal neurons on flat substrates, a polarized morphology gradually establishes after 48 to 72 h.[47] Neuronal cells cultivated on a crinkled CNT substrate establish a highly polar morphology after just 24 h (Figure 3b). Numerous neurites protrude from the cell body on the crinkled surfaces CNT-PU-50 and CNT-100, whereas cells grown on noncrinkly substrates (PU only and CNT-PU-0%) retained a round, unpolarized morphology. These differences indicate that the mesoscale ridge features of crinkly CNT films are beneficial to neuron development. Others have reported outgrowth of neurites on "flat" noncrinkly CNT films,[23] but crinkly mesoscale ridge morphology in CNT-PU-100 stimulates neurite outgrowth, with an increasing number of neurites and greater extension as compared to CNT-PU-0 (Figure 3b of zoomed-in area and Figure S5 of broader view). Higher-resolution SEM images (Figure 3c) also support the conclusion that mesoscale CNT ridge features stimulate polarization. We speculate that neuron polarization and

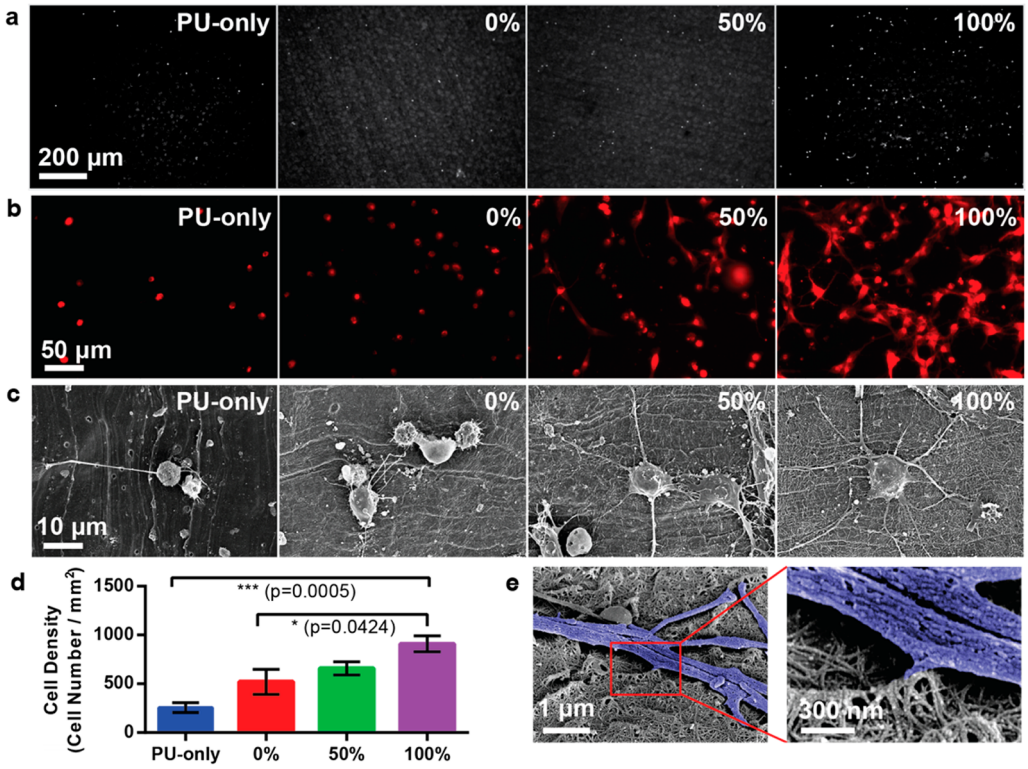

Figure 3. Culturing hippocampal neurons on PU sheets with crinkly CNT thin film. Immunostaining of hippocampal neurons with (a) Hoechst 33342 as nucleus marker for cell counting and (b) CellMask Deep Red as membrane marker for cell morphology visualization on substrates with gradient crinkly morphology (from left to right: PU only, CNT-PU-0, CNT-PU-50, and CNT-PU-100). (c) SEM images of hippocampal neurons cultured on the above substrates. (d) Cell density of the above substrates measured by nucleus staining (error bar: standard error of the mean; *p* value: *t* test). (e) High-magnification SEM images of neurites on CNT-PU-100 substrates (left) and the zoom-in images of its contacting point (right). (Neurite is in pseudocolor.)

axon formation might be stimulated when filopodia extended from unpolarized hippocampal neurons encounter crinkled CNT ridges of similar scale.[48,49] This could explain why neuron cells cultured on crinkled CNT substrates undergo polarization more rapidly than those grown on smooth CNT surfaces. Our speculation is supported by high-resolution SEM images of neuron cells cultured on CNT-PU-100 (Figure 3e), where the neurites connect to crinkled CNT ridges but not to neighboring flat CNTs.

The conductive feature of the CNT networks enables the crinkled CNT thin film to be applied as a bioelectrode in bioelectrochemical systems, such as microbial electrochemical cells. Microbial electrochemical cells convert chemical energy into electrical energy by the catalytic activity of micro-organisms referred to as exoelectrogens.[50−53] Exoelectrogens growing on a bioanode collect electrons by oxidizing electron donors (*e.g.*, glucose) and transfer electrons extracellularly to the bioanode. An affinitive electrode surface with high conductivity and biocompatibility for extracellular electron transfer is essential to bioelectrode performance. The CNT-coated substrates used for the fabrication of bioanodes provides a surface that is attractive for both attachment and collection of electrons.[18]

To investigate the effect of the crinkled CNT films with mesoscale ridge features on extracellular electron transfer, we prepared four different bioelectrode samples, including CNT-PU-100, CNT-PU-50, CNT-PU-0, and PU control. We monitored current over 40 days of operation with these samples as the bioanodes in a traditional H-shaped two-chambered MFC with a platinum cathode for oxygen reduction (Figure 4a). The results indicate that crinkled CNT films improve the collection of electrons from exoelectrogens and enable greater current generation. Bioanodes with crinkled CNT films achieved higher current densities than the CNT-coated PU anode. The charge flow supported by the CNT-PU-50 anode was 38% greater than the CNT-PU-0 anode, and the charge flow supported by the CNT-PU-100 anode was 68% greater. Using linear staircase voltammetry, maximum current densities were 0.9 A/m^2 for the CNT-PU-0 anode, 1.4 A/m^2 for the CNT-PU-50 anode, and 2.4 A/m^2 for the CNT-PU-100 anode. The CNT-PU-50 anode was 1.5-fold higher than the CNT-PU-0 anode, and the CNT-PU-100 anode was 2.6-fold higher (Figure 4b). Maximum current densities of these CNT-coated PU electrodes are comparable to that of the previous reported CNT-coated sponges when normalized to the actual electrode surface.[19]

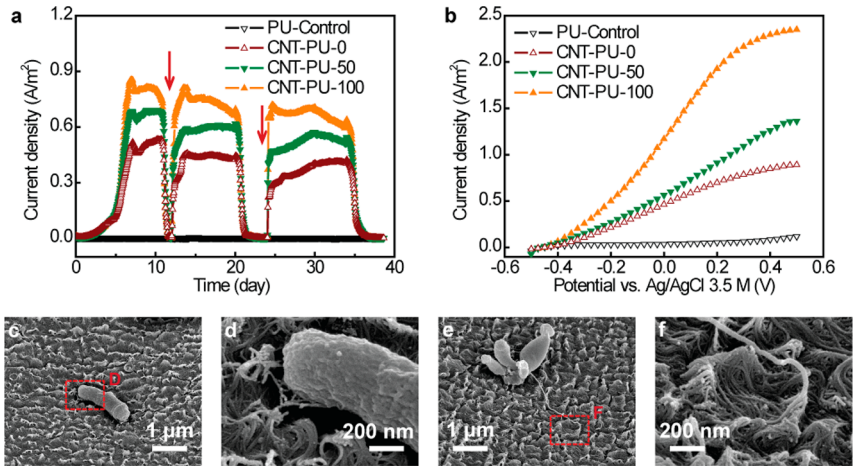

Figure 4. Use of PU sheets with crinkled CNT thin films as anodes in a microbial fuel cell (MFC). The H-shaped two-chambered MFC was inoculated with domestic wastewater and fed a glucose medium (1 g/L). Four anodes include a CNT-coated PU sheet treated with 100% acetone (CNT-PU-100), a CNT-coated PU sheet treated with 50% acetone (CNT-PU-50), an as-prepared CNT-coated PU sheet (CNT-PU-0), and a plain PU control. (a) Current generation of different anodes for 40 days. The red arrows indicate replacement of the glucose medium. The total charge flows achieved by the CNT-PU-100 and CNT-PU-50 are 68 and 38% greater than that achieved by CNT-PU-0. (b) Linear staircase voltammograms of different anodes indicate maximum current densities. Compared to CNT-PU-0, the CNT-PU-100 and CNT-PU-50 achieved 2.6-fold and 1.5-fold higher current output. (c–f) SEM images of micro-organisms on the crinkly CNT thin film, showing strong interaction between the microbial bio-nanowires and the buckled CNT ridge structures.

To investigate the electron transfer properties of different bioanodes, we carried out electrochemical impedance spectroscopy tests.[54] Resistance to electron transfer, as indicated by the semicircle diameter in the Nyquist curves (Figure S6a), was significantly less with crinkled CNT thin films compared to uncrinkled films. Without inoculation, the Nyquist curves for crinkled and uncrinkled films were the same (Figure S6b), but after inoculation, the curves changed, indicating enhanced interaction between exoelectrogens and the crinkly CNT thin film. SEM images indicate that the crinkly CNT thin film morphology is rough and facilitates exoelectrogen attachment, enabling strong interactions with the CNT film (Figure 4c–f and Figure S7). Microbial bio-nanowires and CNT ridge structures at the same scale interconnect to form an integrated network. Bio-nanowires are known to be highly conductive and can directly and efficiently transfer electrons from attached micro-organisms to an electrode.[55–58] Microbial growth was not observed on the plain PU sheet, and the plain PU sheet control anode showed little activity for electron transfer or current generation.

CONCLUSION

We conclude that crinkling of carbon nanotube films by swelling and shrinking of CNT-coated substrates creates mesoscale ridge features (300–500 nm in height and tens of nanometers in width). These features can serve as a useful interface to subcellular components, enhancing cell attachment, growth, differentiation, and electron transfer. We envision a wide range of applications.

EXPERIMENTAL METHODS

Carbon Nanotube Ink Preparation and Coating. Aqueous carbon nanotube ink was prepared by dispersing single-walled CNTs (1 mg/L, Carbon Solutions, Inc., P3-SWNT) in water with sodium dodecylbenzenesulfonate (10 mg/L, Sigma-Aldrich) as a surfactant. The dispersion process includes 5 min of bath sonication and 30 min of probe sonication. Polyurethane sheets or sponges (McMaster-Carr) were first pretreated with oxygen plasma for about 5 min to improve the surface hydrophilicity. Coating CNTs onto PU sheets were conducted by a simple Meyer rod coating method, while CNT-coated PU sponges were prepared by a dipping-and-drying approach.[18,59]

Swelling and Shrinking. To create crinkly morphology of the CNT thin film, CNT-coated PU sheets or sponges were first dipped into an acetone–water solution with various acetone compositions (25, 50, 75, or 100%). The CNT-coated PU sheets or sponges swelled along with time. After equilibrium, they were immerged into deionized water until recovering to their original sizes. Finally, treated PU sheets or sponges were dried in air for more that 24 h. Scanning electron microscope (SEM) images of the CNT thin film before and after the treatments were taken by FEI Nova NanoSEM. Alignment analysis of SEM images was performed using ImageJ with OrientationJ plugin.[60,61] Surface scanning for morphology analysis was done in Park AFM (XE-70) with noncontact mode. The AFM images were analyzed by XEI image processing software. XPS and FT-IR were performed by XPS/ESCA (SSI S-Probe, monochromatized Al Kα radiation at 1486 eV) and Thermo Scientific Nicolet iS50 FT-IR spectrometer, respectively.

Neuron Cell Culture. Embryonic hippocampal neurons were isolated from E18 rats according to previously published protocols[62] and then dissociated and plated on 0.2 mg/mL poly-L-lysine-coated CNT films, where the CNT films were presterilized in 70% ethanol. After being maintained in neurobasal medium supplemented with B27 and L-glutamine for 24 h, the neurons were stained by CellMask Deep Red and Hoechst 33342 and then fixed by 4% paraformaldehyde. Optical and fluorescent images were taken by Leica DMI6000 B microscope. Samples for SEM were pretreated by a fixing and critical point drying process[18] and imaged by field emission scanning electron microscope (FEI Nova NanoSEM).

Microbial Fuel Cell Setup, Operation, and Characterization. A traditional H-shaped two-chambered microbial fuel cell was constructed as described previously.[18] Four anode samples (1 cm × 1 cm), including a CNT-coated PU sheet treated with 100% acetone (CNT-PU-100), a CNT-coated PU sheet treated with 50% acetone (CNT-PU-50), an as-prepared CNT-coated PU sheet (CNT-PU-0), and a plain PU control, were tested simultaneously in the same anode chamber. Stainless steel meshes were applied as current collectors. The cathode was carbon cloth (2 cm × 5 cm, projected area of 20 cm^2, Fuel Cell Earth LLC, MA) with a catalyst layer (0.5 mg/cm^2 10 wt % Pt on XC-72). The MFC was inoculated with domestic wastewater from the Palo Alto Regional Water Quality Control Plant and fed a glucose solution (1 g/L). The anolyte was replaced when the current production was significantly declined, indicating the depletion of glucose. Voltages across 1 kΩ external resistors were recorded. Electrochemical characterizations on the four anodes (WE) were carried out using a BioLogic VMP3 potentiostat−galvanostat. The counter electrode was Pt, and the reference electrode (RE) was a double junction Ag|AgCl|KCl (3.5M) electrode. Linear staircase voltammetries were applied by increase the WE potential from −0.5 to 0.5 V *vs* RE by 25 mV each time and recording the current after 3 min for equilibrium. Electrochemical impedance spectroscopy tests were conducted at the OCV in the frequency range of 10^5 to 0.1 Hz with a 10 mV peak-to-peak sinusoidal potential perturbation, and the results were reported as Nyquist plots. Anode samples for SEM were pretreated by a fixing and critical point drying process[18] and explored by FEI Nova NanoSEM.

Conflict of Interest: The authors declare no competing financial interest.

Acknowledgment. X.X. acknowledges support from a Stanford Interdisciplinary Graduate Fellowship. M.Y. acknowledges support from the Woods Institute for the Environment at Stanford University.

Supporting Information Available: Supplementary figures. This material is available free of charge *via* the Internet at http://pubs.acs.org.

REFERENCES AND NOTES

1. Gasiorowski, J. Z.; Murphy, C. J.; Nealey, P. F. Biophysical Cues and Cell Behavior: The Big Impact of Little Things. *Annu. Rev. Biomed. Eng.* **2013**, *15*, 155–176.
2. Kim, H. N.; Jiao, A.; Hwang, N. S.; Kim, M. S.; Do Hyun, K.; Kim, D.-H.; Suh, K.-Y. Nanotopography-Guided Tissue Engineering and Regenerative Medicine. *Adv. Drug Delivery Rev.* **2013**, *65*, 536–558.
3. Kim, W.; Ng, J. K.; Kunitake, M. E.; Conklin, B. R.; Yang, P. Interfacing Silicon Nanowires with Mammalian Cells. *J. Am. Chem. Soc.* **2007**, *129*, 7228–7229.
4. Chen, W.; Weng, S.; Zhang, F.; Allen, S.; Li, X.; Bao, L.; Lam, R. H. W.; Macoska, J. A.; Merajver, S. D.; Fu, J. Nanoroughened Surfaces for Efficient Capture of Circulating Tumor Cells without Using Capture Antibodies. *ACS Nano* **2013**, *7*, 566–575.
5. Chen, W.; Villa-Diaz, L. G.; Sun, Y.; Weng, S.; Kim, J. K.; Lam, R. H. W.; Han, L.; Fan, R.; Krebsbach, P. H.; Fu, J. Nanotopography Influences Adhesion, Spreading, and Self-Renewal of Human Embryonic Stem Cells. *ACS Nano* **2012**, *6*, 4094–4103.
6. Xie, C.; Hanson, L.; Xie, W.; Lin, Z.; Cui, B.; Cui, Y. Noninvasive Neuron Pinning with Nanopillar Arrays. *Nano Lett.* **2010**, *10*, 4020–4024.
7. Jeong, H. E.; Kim, I.; Karam, P.; Choi, H.-J.; Yang, P. Bacterial Recognition of Silicon Nanowire Arrays. *Nano Lett.* **2013**, *13*, 2864–2869.
8. Bucaro, M. A.; Vasquez, Y.; Hatton, B. D.; Aizenberg, J. Fine-Tuning the Degree of Stem Cell Polarization and Alignment on Ordered Arrays of High-Aspect-Ratio Nanopillars. *ACS Nano* **2012**, *6*, 6222–6230.
9. Fan, L.; Feng, C.; Zhao, W.; Qian, L.; Wang, Y.; Li, Y. Directional Neurite Outgrowth on Superaligned Carbon Nanotube Yarn Patterned Substrate. *Nano Lett.* **2012**, *12*, 3668–3673.
10. Xie, J.; Liu, W.; MacEwan, M. R.; Bridgman, P. C.; Xia, Y. Neurite Outgrowth on Electrospun Nanofibers with Uniaxial Alignment: The Effects of Fiber Density, Surface Coating, and Supporting Substrate. *ACS Nano* **2014**, *8*, 1878–1885.
11. Hochbaum, A. I.; Aizenberg, J. Bacteria Pattern Spontaneously on Periodic Nanostructure Arrays. *Nano Lett.* **2010**, *10*, 3717–3721.
12. Epstein, A. K.; Hochbaum, A. I.; Kim, P.; Aizenberg, J. Control of Bacterial Biofilm Growth on Surfaces by Nanostructural Mechanics and Geometry. *Nanotechnology* **2011**, *22*, 494007.
13. Teo, B. K. K.; Wong, S. T.; Lim, C. K.; Kung, T. Y. S.; Yap, C. H.; Ramagopal, Y.; Romer, L. H.; Yim, E. K. F. Nanotopography Modulates Mechanotransduction of Stem Cells and Induces Differentiation through Focal Adhesion Kinase. *ACS Nano* **2013**, *7*, 4785–4798.
14. Cho, W. K.; Kang, K.; Kang, G.; Jang, M. J.; Nam, Y.; Choi, I. S. Pitch-Dependent Acceleration of Neurite Outgrowth on Nanostructured Anodized Aluminum Oxide Substrates. *Angew. Chem., Int. Ed.* **2010**, *49*, 10114–10118.
15. Migliorini, E.; Grenci, G.; Ban, J.; Pozzato, A.; Tormen, M.; Lazzarino, M.; Torre, V.; Ruaro, M. E. Acceleration of Neuronal Precursors Differentiation Induced by Substrate Nanotopography. *Biotechnol. Bioeng.* **2011**, *108*, 2736–2746.
16. Wang, S.; Wang, H.; Jiao, J.; Chen, K.-J. J.; Owens, G. E.; Kamei, K.-I.; Sun, J.; Sherman, D. J.; Behrenbruch, C. P.; Wu, H.; *et al.* Three-Dimensional Nanostructured Substrates toward Efficient Capture of Circulating Tumor Cells. *Angew. Chem., Int. Ed.* **2008**, *48*, 8970–8973.
17. Fischer, K. E.; Alemán, B. J.; Tao, S. L.; Hugh Daniels, R.; Li, E. M.; Bünger, M. D.; Nagaraj, G.; Singh, P.; Zettl, A.; Desai, T. A. Biomimetic Nanowire Coatings for Next Generation Adhesive Drug Delivery Systems. *Nano Lett.* **2009**, *9*, 716–720.
18. Xie, X.; Hu, L.; Pasta, M.; Wells, G. F.; Kong, D.; Criddle, C. S.; Cui, Y. Three-Dimensional Carbon Nanotube-Textile Anode for High-Performance Microbial Fuel Cells. *Nano Lett.* **2011**, *11*, 291–296.
19. Xie, X.; Ye, M.; Hu, L.; Liu, N.; McDonough, J. R.; Chen, W.; Alshareef, H. N.; Criddle, C. S.; Cui, Y. Carbon Nanotube-Coated Macroporous Sponge for Microbial Fuel Cell Electrodes. *Energy Environ. Sci.* **2012**, *5*, 5265–5270.
20. Scardino, A. J.; Zhang, H.; Cookson, D. J.; Lamb, R. N.; de Nys, R. The Role of Nano-Roughness in Antifouling. *Biofouling* **2009**, *25*, 757–767.
21. Albuschies, J.; Vogel, V. The Role of Filopodia in the Recognition of Nanotopographies. *Sci. Rep.* **2013**, *3*, 1658.
22. Friedlander, R. S.; Vlamakis, H.; Kim, P.; Khan, M.; Kolter, R.; Aizenberg, J. Bacterial Flagella Explore Microscale Hummocks and Hollows To Increase Adhesion. *Proc. Natl. Acad. Sci. U.S.A.* **2013**, *110*, 5624–5629.
23. Hu, H.; Ni, Y.; Montana, V.; Haddon, R. C.; Parpura, V. Chemically Functionalized Carbon Nanotubes as Substrates for Neuronal Growth. *Nano Lett.* **2004**, *4*, 507–511.
24. Lovat, V.; Pantarotto, D.; Lagostena, L.; Cacciari, B.; Grandolfo, M.; Righi, M.; Spalluto, G.; Prato, M.; Ballerini, L. Carbon Nanotube Substrates Boost Neuronal Electrical Signaling. *Nano Lett.* **2005**, *5*, 1107–1110.
25. Baik, K. Y.; Park, S. Y.; Heo, K.; Lee, K. B.; Hong, S. Carbon Nanotube Monolayer Cues for Osteogenesis of Mesenchymal Stem Cells. *Small* **2011**, *7*, 741–745.
26. Kim, J. A.; Jang, E. Y.; Kang, T. J.; Yoon, S.; Ovalle-Robles, R.; Rhee, W. J.; Kim, T.; Baughman, R. H.; Kim, Y. H.; Park, T. H. Regulation of Morphogenesis and Neural Differentiation of Human Mesenchymal Stem Cells Using Carbon Nanotube Sheets. *Integr. Biol.* **2012**, *4*, 587–594.
27. Zhang, X.; Prasad, S.; Niyogi, S.; Morgan, A.; Ozkan, M.; Ozkan, C. Guided Neurite Growth on Patterned Carbon Nanotubes. *Sens. Actuators, B* **2005**, *106*, 843–850.
28. Cellot, G.; Cilia, E.; Cipollone, S.; Rancic, V.; Sucapane, A.; Giordani, S.; Gambazzi, L.; Markram, H.; Grandolfo, M.;

Scaini, D.; *et al.* Carbon Nanotubes Might Improve Neuronal Performance by Favouring Electrical Shortcuts. *Nat. Nanotechnol.* **2009**, *4*, 126–133.
29. Keefer, E. W.; Botterman, B. R.; Romero, M. I.; Rossi, A. F.; Gross, G. W. Carbon Nanotube Coating Improves Neuronal Recordings. *Nat. Nanotechnol.* **2008**, *3*, 434–439.
30. Jang, M. J.; Namgung, S.; Hong, S.; Nam, Y. Directional Neurite Growth Using Carbon Nanotube Patterned Substrates as a Biomimetic Cue. *Nanotechnology* **2010**, *21*, 235102.
31. Hu, L.; Hecht, D. S.; Grüner, G. Carbon Nanotube Thin Films: Fabrication, Properties, and Applications. *Chem. Rev.* **2010**, *110*, 5790–5844.
32. Ren, Z.; Huang, Z.; Xu, J.; Wang, J.; Bush, P.; Siegal, M.; Provencio, P. Synthesis of Large Arrays of Well-Aligned Carbon Nanotubes on Glass. *Science* **1998**, *282*, 1105–1107.
33. Wu, Z.; Chen, Z.; Du, X.; Logan, J. M.; Sippel, J.; Nikolou, M.; Kamaras, K.; Reynolds, J. R.; Tanner, D. B.; Hebard, A. F.; *et al.* Transparent, Conductive Carbon Nanotube Films. *Science* **2004**, *305*, 1273–1276.
34. Lin, P.-C.; Yang, S. Spontaneous Formation of One-Dimensional Ripples in Transit to Highly Ordered Two-Dimensional Herringbone Structures through Sequential and Unequal Biaxial Mechanical Stretching. *Appl. Phys. Lett.* **2007**, *90*, 241903.
35. Xu, F.; Wang, X.; Zhu, Y.; Zhu, Y. Wavy Ribbons of Carbon Nanotubes for Stretchable Conductors. *Adv. Funct. Mater.* **2012**, *22*, 1279–1283.
36. Yu, C.; Masarapu, C.; Rong, J.; Wei, B.; Jiang, H. Stretchable Supercapacitors Based on Buckled Single-Walled Carbon-Nanotube Macrofilms. *Adv. Mater.* **2009**, *21*, 4793–4797.
37. Oberth, A. E. Equilibrium Swelling of Polyurethane Elastomers. *Rubber Chem. Technol.* **1990**, *63*, 56–65.
38. Harogoppad, S. B.; Aithal, U. S.; Aminabhavi, T. M. Diffusion of Organic-Solvents into Polyurethane Network from Swelling Measurements. *J. Appl. Polym. Sci.* **1991**, *42*, 3267–3270.
39. Jiang, H.; Khang, D.-Y.; Fei, H.; Kim, H.; Huang, Y.; Xiao, J.; Rogers, J. A. Finite Width Effect of Thin-Films Buckling on Compliant Substrate: Experimental and Theoretical Studies. *J. Mech. Phys. Solids* **2008**, *56*, 2585–2598.
40. Jia, H.; Wang, S.; Goudeau, P.; Li, L.; Xue, X. Investigation of Buckling Transition from Straight-Sided to Telephone-Cord Wrinkles in Al Films. *J. Micromech. Microeng.* **2013**, *23*, 045014.
41. Kotov, N. A.; Winter, J. O.; Clements, I. P.; Jan, E.; Timko, B. P.; Campidelli, S.; Pathak, S.; Mazzatenta, A.; Lieber, C. M.; Prato, M.; *et al.* Nanomaterials for Neural Interfaces. *Adv. Mater.* **2009**, *21*, 3970–4004.
42. Voge, C. M.; Stegemann, J. P. Carbon Nanotubes in Neural Interfacing Applications. *J. Neural Eng.* **2011**, *8*, 011001.
43. Bosi, S.; Fabbro, A.; Ballerini, L.; Prato, M. Carbon Nanotubes: A Promise for Nerve Tissue Engineering? *Nanotechnol. Rev.* **2013**, *2*, 47–57.
44. Galvan-Garcia, P.; Keefer, E. W.; Yang, F.; Zhang, M.; Fang, S.; Zakhidov, A. A.; Baughman, R. H.; Romero, M. I. Robust Cell Migration and Neuronal Growth on Pristine Carbon Nanotube Sheets and Yarns. *J. Biomater. Sci., Polym. Ed* **2007**, *18*, 1245–1261.
45. Cellot, G.; Toma, F. M.; Varley, Z. K.; Laishram, J.; Villari, A.; Quintana, M.; Cipollone, S.; Prato, M.; Ballerini, L. Carbon Nanotube Scaffolds Tune Synaptic Strength in Cultured Neural Circuits: Novel Frontiers in Nanomaterial−Tissue Interactions. *J. Neurosci.* **2011**, *31*, 12945–12953.
46. Béduer, A.; Seichepine, F.; Flahaut, E.; Loubinoux, I.; Vaysse, L.; Vieu, C. Elucidation of the Role of Carbon Nanotube Patterns on the Development of Cultured Neuronal Cells. *Langmuir* **2012**, *28*, 17363–17371.
47. Barnes, A. P.; Polleux, F. Establishment of Axon-Dendrite Polarity in Developing Neurons. *Annu. Rev. Neurosci.* **2009**, *32*, 347–381.
48. Bugnicourt, G.; Brocard, J.; Nicolas, A.; Villard, C. Nanoscale Surface Topography Reshapes Neuronal Growth in Culture. *Langmuir* **2014**, *30*, 4441–4449.
49. Kang, K.; Yoon, S. Y.; Choi, S.-E.; Kim, M.-H.; Park, M.; Nam, Y.; Lee, J. S.; Choi, I. S. Cytoskeletal Actin Dynamics Are Involved in Pitch-Dependent Neurite Outgrowth on Bead Monolayers. *Angew. Chem., Int. Ed.* **2014**, *53*, 6075–6079.
50. Logan, B. E.; Hamelers, B.; Rozendal, R. A.; Schrorder, U.; Keller, J.; Freguia, S.; Aelterman, P.; Verstraete, W.; Rabaey, K. Microbial Fuel Cells: Methodology and Technology. *Environ. Sci. Technol.* **2006**, *40*, 5181–5192.
51. Logan, B. E. Exoelectrogenic Bacteria That Power Microbial Fuel Cells. *Nat. Rev. Microbiol.* **2009**, *7*, 375–381.
52. Lovley, D. R. Bug Juice: Harvesting Electricity with Microorganisms. *Nat. Rev. Microbiol.* **2006**, *4*, 497–508.
53. Lovley, D. R. Electromicrobiology. *Annu. Rev. Microbiol.* **2012**, *66*, 391–409.
54. He, Z.; Mansfeld, F. Exploring the Use of Electrochemical Impedance Spectroscopy (EIS) in Microbial Fuel Cell Studies. *Energy Environ. Sci.* **2009**, *2*, 215–219.
55. Reguera, G.; McCarthy, K. D.; Mehta, T.; Nicoll, J. S.; Tuominen, M. T.; Lovley, D. R. Extracellular Electron Transfer *via* Microbial Nanowires. *Nature* **2005**, *435*, 1098–1101.
56. Gorby, Y. A.; Yanina, S.; McLean, J. S.; Rosso, K. M.; Moyles, D.; Dohnalkova, A.; Beveridge, T. J.; Chang, I. S.; Kim, B. H.; Kim, K. S.; *et al.* Electrically Conductive Bacterial Nanowires Produced by Shewanella Oneidensis Strain MR-1 and Other Microorganisms. *Proc. Natl. Acad. Sci. U.S.A.* **2006**, *103*, 11358–11363.
57. Jiang, X.; Hu, J.; Fitzgerald, L. A.; Biffinger, J. C.; Xie, P.; Ringeisen, B. R.; Lieber, C. M. Probing Electron Transfer Mechanisms in *Shewanella oneidensis* MR-1 Using a Nanoelectrode Platform and Single-Cell Imaging. *Proc. Natl. Acad. Sci. U.S.A.* **2010**, *107*, 16806–16810.
58. El-Naggar, M. Y.; Wanger, G.; Leung, K. M.; Yuzvinsky, T. D.; Southam, G.; Yang, J.; Lau, W. M.; Nealson, K. H.; Gorby, Y. A. Electrical Transport along Bacterial Nanowires from *Shewanella oneidensis* MR-1. *Proc. Natl. Acad. Sci. U.S.A.* **2010**, *107*, 18127–18131.
59. Hu, L.; Choi, J. W.; Yang, Y.; Jeong, S.; La Mantia, F.; Cui, L.-F.; Cui, Y. Highly Conductive Paper for Energy-Storage Devices. *Proc. Natl. Acad. Sci. U.S.A.* **2009**, *106*, 21490–21494.
60. Schneider, C. A.; Rasband, W. S.; Eliceiri, K. W. NIH Image to ImageJ: 25 Years of Image Analysis. *Nat. Methods* **2012**, *9*, 671–675.
61. Rezakhaniha, R.; Agianniotis, A.; Schrauwen, J. T. C.; Griffa, A.; Sage, D.; Bouten, C. V. C.; Vosse, F. N.; Unser, M.; Stergiopulos, N. Experimental Investigation of Collagen Waviness and Orientation in the Arterial Adventitia Using Confocal Laser Scanning Microscopy. *Biomech. Model. Mechanobiol.* **2011**, *11*, 461–473.
62. Fath, T.; Ke, Y. D.; Gunning, P.; Götz, J.; Ittner, L. M. Primary Support Cultures of Hippocampal and Substantia Nigra Neurons. *Nat. Protoc.* **2009**, *4*, 78–85.